J Solid State Electrochem (2010) 14:241–248
DOI 10.1007/s10008-009-0806-5

ORIGINAL PAPER

CdSe electrodeposition on anodic, barrier or porous Ti oxides. A sensitization effect

T. Kosanovic · D. Karoussos · M. Bouroushian

Received: 30 December 2008 / Revised: 12 February 2009 / Accepted: 16 February 2009 / Published online: 12 March 2009

Abstract A variety of oxide layers, from passive amorphous TiO_x of few nanometer thicknesses to micrometer-thick porous with different anatase to rutile ratios, were prepared by potentiostatic or galvanostatic anodization of Ti metal in H_2SO_4 and HF/H_3PO_4 solutions and used as substrates for electrodeposition of cadmium selenide from acidic selenite baths. The substrate and CdSe microstructures were investigated by X-ray diffraction and electron microscopy techniques. Barrier TiO_x and heterogeneously structured oxide substrates induced growth of zinc blend/wurtzite CdSe, whereas highly ordered porous titanium dioxide (TiO_2) accommodated growth of (10.0) oriented hexagonal CdSe thin layers. Pulsed potential plating was employed to control pore-filling during electrodeposition of CdSe. Photoelectrochemical evaluation of the produced electrodes in polysulfide cell under green light illumination implied a TiO_2 sensitization effect in the case of CdSe/(porous TiO_2)/Ti system, as evidenced by a negative shift in flat band potential and an increase in open circuit potential. The sensitization effect was observed even with CdSe deposited by a single potential pulse signifying the importance of contacting the TiO_2 surface to the electrolytic solution via a very thin layer of CdSe.

Keywords Optical sensitization · Titanium dioxide · Cadmium selenide · Anodization · Electrodeposition · Photoelectrochemistry

T. Kosanovic (✉) · D. Karoussos · M. Bouroushian
General Chemistry Laboratory, School of Chemical Engineering,
National Technical University of Athens,
9 Heroon Polytechniou str., Zografos Campus,
157 73 Athens, Greece
e-mail: kosanot@central.ntua.gr

Introduction

Titanium dioxide (TiO_2) is a particularly versatile material used in a variety of applications such as solar cells, photocatalytic electrodes, gas sensors, structural ceramics, and biocompatible materials. As a semiconductor, TiO_2 absorbs light only in the UV region (indirect band gap at ca. 3.2 eV), and for that reason, a variety of materials such as organic dyes and lower gap semiconductors have been used as sensitizers to expand its photoactivity in the visible. Dye-sensitized TiO_2 nanostructured electrodes are used in state-of-the-art solar cells with high energy conversion efficiency (11%), long time stability, and low cost production [1, 2].

Gerischer and Lübke [3] were the first to suggest the use of an inorganic semiconductor (CdS, E_g=2.4 eV) obtained by chemical deposition on TiO_2, as an alternative to organic dye sensitizers, but since then (1986), little work has been done in this field. Recently, sensitization based on chalcogenide compounds has attracted renewed interest. Different TiO_2 morphologies, from polycrystalline to nanostructured powder and thin films, have been photosensitized by the introduction of chalcogenides, in particular CdSe (direct band gap of 1.7 eV), commonly by employing chemical bath deposition [4–8]. For instance, CdSe-sensitized porous TiO_2 photoanodes were used in photoelectrochemical cells (PEC) [5], while CdSe quantum dots (QDs) deposited on nanostructured TiO_2 electrodes with different rutile (R)/anatase (A) ratios were shown to yield an effective sensitization result. In particular, it was suggested that rutile TiO_2 mixing is advantageous in improving the photoelectrochemical properties of the electrode. A red shift in the light absorption limit was observed upon increasing the quantity of CdSe-QDs on TiO_2 [6]. Moreover, nanostructured TiO_2 and uniform TiO_2 nanotube arrays fabricated on Ti substrates have been effectively sensitized by CdSe-QDs [7, 8].

Electrochemical anodization of metallic Ti in an acidic solution can be advantageously used for the preparation of thin TiO_x films, on account of the precise growth control that can be achieved via the applied potential or current; further, a good ohmic contact with the underlying metal is immediately formed upon anodization [9–18]. Thick anodic films formed at potentials greater than 50 V have very similar properties to bulk crystalline TiO_2 in terms of electronic behavior [9, 10]. Various approaches for Ti anodization have been addressed, producing a variety of oxide forms, ranging from passive microstructured and nanostructured thin TiO_x/Ti films prepared in sulfuric acid [10–12] to self-organized TiO_2 nanotubes obtained from a variety of aqueous [13–16] and nonaqueous electrolytes [17, 18]. Note that titanium dioxide has three naturally occurring crystal phases: rutile, anatase, and brookite (B). The former two adopt a tetragonal structure while brookite is orthorhombic. All three are made up of differing arrays of distorted TiO_6 octahedra. Rutile is the thermodynamically stable polymorph at all temperatures and pressures, while anatase and brookite are kinetically controlled phases. Each crystalline modification has different physicochemical properties, such as density, refractive index, and photochemical reactivity.

In this work, we present an investigation on the electrochemical preparation and properties of anodic titanium oxide/Ti electrodes and their sensitization by electrodeposition of CdSe. The objective was to establish an intimate contact of large interface area between CdSe and the oxide substrate. Changes in size, distribution, and crystal structure of the CdSe crystallites that could be attributed to substrate-induced effects have been detected. Further, equilibrium and operating properties of the as-prepared electrodes in PECs with a sulfide polysulfide redox electrolyte were determined.

Experimental

Commercially pure Ti electrodes (discs ∅ 12 mm, ASTM Grade-2) were used as substrates. The specimens were mechanically abraded with SiC paper (grades 400–2,500), polished by 0.3 μm grain size alumina powder and sonicated in 10% ethanol and water. Prior to each anodization, Ti substrates were etched by a 10% HF solution for 10 s in order to remove the native superficial oxide film, ultrasonically rinsed, and dried in a nitrogen stream.

The anodic oxidation process took place in a two electrode cell, with Ti as the anode and stainless steel as the cathode, at room temperature, while a direct current power supply was used to provide different electric potentials, or currents between the two electrodes, defining potentiostatic or galvanostatic control. The working electrolyte composition, anodization potential/current (E_A/I_A), and anodization time (t_A) are summarized in Table 1. In all potentiostatic processes, the anodization potential was slowly swept from 0 V to the final value within 1 min and kept there for the desirable time. After anodization, the samples were rinsed with ultrapure water and dried in a stream of N_2.

CdSe was grown on the oxide substrates using the typical acidic aqueous electrochemical method [19, 20]. The electrodeposition took place in a thermostat-controlled conventional three-electrode cell (Pt grid counter and Hg/Hg_2SO_4 saturated sulfate reference (SSE)) at 85–90 °C, by using a potentioscan (Wenking PGS 81R) system coupled to a pulse generator (Wenking DPC 72). A rotating disc working electrode was employed in order to control the mass transfer regime in the electrolytic solution. There was no correction for ohmic drop. Water (18.3 MΩ cm), purified by an ultrapure water system (Easy Pure Barnstead RF), as received analytical grade selenite (SeO_2) and $3CdSO_4 \times 8H_2O$ reagents were used for the preparation of experimental solutions with final concentrations of 1×10^{-3} and 0.2 M, respectively. The bath pH was adjusted by sulfuric acid to 1.9 at the working temperature. Electrodeposition was carried out either at a constant potential of $E = -0.9$ V vs. SSE or by imposing an alternating double signal of rectangular-controlled potential between 0 V and −0.9 vs. SSE with a duty cycle (d.c.) between 12.5% and 87.5% and a frequency of 0.25 Hz. The total electrolysis charge for each deposition was between 0.2 to 4 C.

The oxide substrate and CdSe epilayer were studied by means of solid state techniques, i.e., scanning electron microscope (SEM) equipped with energy-dispersive X-ray (EDAX) elemental analysis by FEI Quanta 200, conventional Bragg-Brentano (X-ray diffraction, XRD) and low-angle incidence X-ray diffraction (LIXD) by a Siemens D5000 powder unit with Cu-K_α source. In LIXD, the depth profile analysis of the films is carried out by controlling the

Table 1 Treatments and "types" of anodized substrate

E_A/I_A	t_A (h)	Electrolyte	Anodization "type"
5, 10, 20, 50, 75, 100 V	¼–2	1 M H_2SO_4	P_1
5 or 10 mA cm^{-2}	1–3	1 M H_2SO_4	G
20, 40 V	½–72	1 M H_3PO_4 0.5% HF	P_2

glancing incidence angle α of the X-rays. Setting the α angle at low values, the path of the X-rays through regions closer to the surface is considerably increased, giving rise to relatively stronger reflections from these regions, at the expense of signals from regions more distant to the surface.

The photoelectrochemical properties of as-prepared electrodes were tested in a sulfide–polysulfide (1 M NaOH, 1 M Na_2S, 1 M S) electrolyte, by means of standard photocurrent–potential measurements. Linear sweep photocurrent voltammetry (10 mV s^{-1}) was applied using a potentioscan system (Wenking PGS 81R) in a single compartment three-electrode cell (Pt counter and pseudoreference), thermostat controlled at 23 °C, under green light illumination obtained by interposing a dichroic filter between the cell and a halogen lamp source (100 mW cm^{-2}). Photocurrent-spectroscopy measurements were also carried out in a two-electrode (Pt counter) microcell, illuminated through a Carl-Zeiss monochromator by a 150-W discharge metal-halides source (color temperature 4,200 K). All measurements were obtained by a computer-controlled recording system using a nA-sensitive current-to-voltage converter.

Results and discussion

Potentiostatic anodization of Ti and electrodeposition of CdSe

Barrier titanium oxides are obtained by potentiostatic anodization (Table 1, P_1) of titanium metal in a sulfuric acid electrolyte. Electrodes anodized at a very low potential (E_A=5 V) for relatively short times (t_A=15 min) show only XRD reflections corresponding to the metal substrate, suggesting that any formed Ti-oxide layer is in an amorphous state (Fig. 1a). As the anodization voltage increases from 10 to 100 V, the oxide gradually transforms to quasicrystalline, as indicated by the observed rutile, brookite, and anatase reflections. Aging of thin films at the applied voltage leads to a higher degree of oxide crystallinity. Evidently, sharp and distinct reflections of (101) anatase and (110) rutile are obtained at E_A=100 V for t_A= 2 h (Fig. 1b). A phase transition from brookite to anatase and rutile TiO_2 is also detected. In general, a higher anodization voltage of Ti is needed to achieve a higher degree of TiO_2 crystallization. The different crystalline phase content ratios in anodized samples were estimated according to the method of Zhang and Banfield [21] involving the integrated XRD intensities of anatase (101), rutile (110), and brookite (121) peaks. The calculated contents of anatase (A), rutile (R), and brookite (B) for crystallized phases have been included along with the corresponding diagrams in Fig. 1.

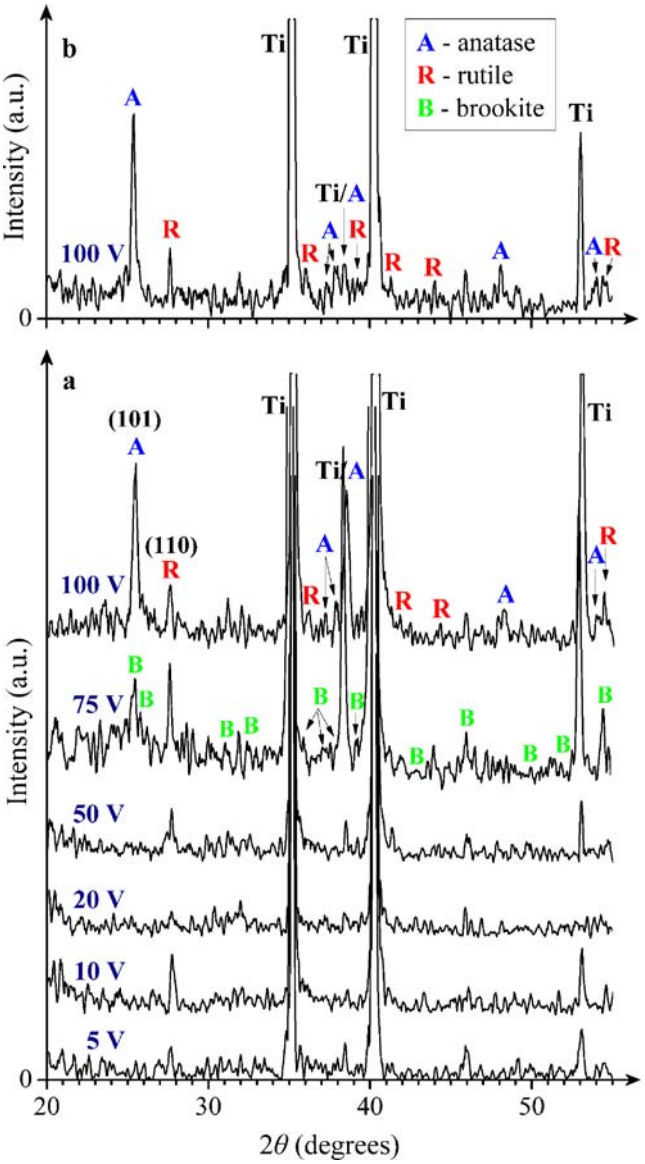

Fig. 1 X-ray patterns of oxides obtained on Ti (P_1) at various potentials from a 1-M H_2SO_4 bath at 25 °C. Anodization time: **a** 15 min; **b** 2 h. JCPDS standards nos. 21-1276, 29-1360, and 21-1272 were used for rutile, brookite, and anatase phase identification. The estimated A/B/R content ratios in anodized films obtained at 50 V for 15 min were 7:51:42% A/R/B, at 75 V for 15 min—30:44:26% A/R/B, at 100 V for 15 min—66:17:17% A/R/B, and at 100 V for 2 h—80:20% A/R

Further identification of the microstructure of "amorphous" oxides, down to very thin surface layers, was achieved by LIXD which allowed the detection of titanium suboxides (e.g., Ti_2O, Ti_2O_3). These deficient in oxygen titanium oxides were found in the layers obtained at low anodization potentials, e.g., E_A=5 V in Fig. 2.

The morphology of the anodized Ti substrates, the topology of the oxide pits/pores, their size, and distribution were studied by SEM. At low anodization potentials, crack-free uniform films are obtained reproducing perfectly the

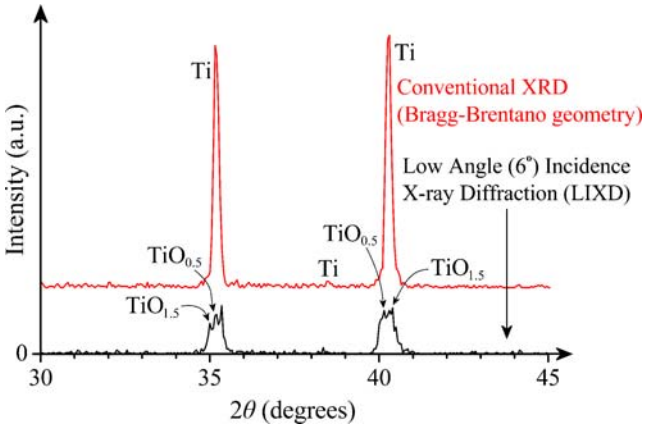

Fig. 2 Conventional and low incidence angle X-ray patterns of oxide layer obtained on Ti (P_1) at E_A=5 V from a 1-M H_2SO_4 bath at 25°C for 15 min. JCPDS nos. 10-0063 and 11-0218 were used for Ti_2O and Ti_2O_3 identification

Ti substrate. However, at high potentials (E_A>50 V), a different morphology develops manifested by crater-like forms bursting out of the surface (Fig. 3a). The change in the morphology is connected to the so-called dielectric breakdown of the oxide film [11].

In general, the oxides grown from sulfuric acid without HF (Table 1, P_1) at constant voltages are compact and thin while their thickness increases linearly with the applied voltage [10, 13]. For a constant potential, the anodic oxide forming rate decreases with time due to the rise of electric resistance. The film crystallizes progressively rather than gaining thickness.

In order to estimate the thickness of the obtained oxides, a depth profile analysis by LIXD was carried out according to the method suggested by Nauer et al. [22]. Normalized theoretical diffraction intensities of rutile and anatase versus the glancing angle α of the incident X-ray beam were simulated for a series of oxide thickness values d=50–1,000 nm. The angle of incidence α was set to different values (0.2–10°) in order to vary the interaction length in each depth region. Measured and corrected anatase (101) or rutile (110) diffraction intensities were fitted to the simulated curves for various α-angles. The estimated thickness of, e.g., the film grown at 100 V is 400 nm, corresponding to a growth rate of 4 nm V^{-1} which is close to the referred value of 2.5 nm V^{-1} for potentiostatic anodic Ti films produced in 0.5 M H_2SO_4 [10].

Variant microstructures of CdSe films were formed on these Ti barrier oxide substrates by typical electrodeposition from an acidic selenite bath [19, 20]. The obtained layers were polycrystalline, consisting of randomly oriented cubic blend as well as a small amount of wurtzite CdSe crystallites (ref. JCPDS cards nos. 19-0191 and 08-0459). XRD profiling by the Debye–Scherrer technique showed crystallite sizes in the range of 25 to 90 nm depending on the substrate microstructure as determined by anodization potential (Fig. 4). According to EDAX analysis, a 5–10% excess of Se, easily removed by low temperature annealing or photoetching, was observed in the as-deposited films.

The growth of CdSe crystallites could be described by the following model: At low anodization voltages, a thin Ti oxide film is formed with a lower oxygen content (according to LIXD: Ti_2O_3, Ti_3O_5) providing numerous active sites for CdSe nucleation (Scheme 1). In this case the limitation of CdSe clusters growth due to lateral overlapping gives rise to the formation of relatively small crystallites. CdSe obtains a defective structure and deviates from the equilibrium cubic symmetry and the hexagonal phase appears. The increasing passivity of the Ti surface due to the formation of mostly amorphous TiO_x results in a smaller number of active nucleation sites, thus leading to an undisturbed growth of larger CdSe crystallites (Scheme 1). The breakdown of the oxide film and the subsequent structural change provide a surface prone to multiple nucleation due to conductive pits. The recrystallization of the oxide, "healing" the surface, results once more in the

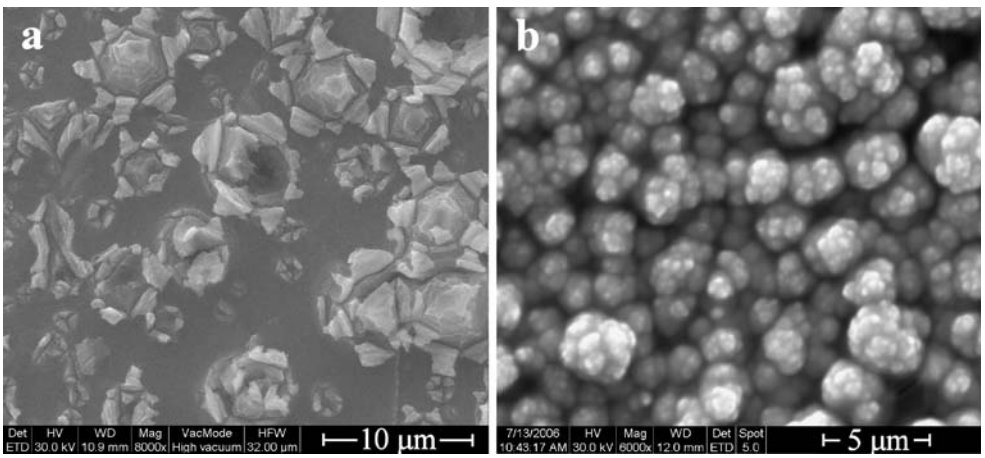

Fig. 3 SEM micrographs of **a** the oxide substrate obtained at E_A=75 V, t_A=2 h and **b** CdSe epilayer prepared at −0.9 V from a typical selenite bath. XRD crystallite size of CdSe is 50 nm

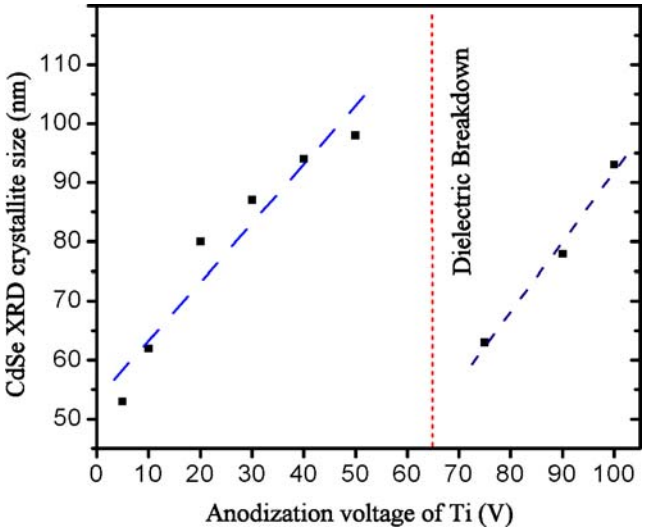

Fig. 4 XRD crystallite size of CdSe deposited at −0.9 V from a 1×10^{-3}-M in SeO_2 and 0.2-M $CdSO_4$ typical bath vs. oxidation voltage of the titanium substrate anodized in 1 M H_2SO_4 for 15 min

decrease of active sites, leading to larger CdSe crystallites (Fig. 4; Scheme 1). The surface density of active centers competes with the anatase layer coverage. As shown in Fig. 3b, open cauliflower CdSe grains having a similar diameter as the breakdown craters were observed on substrates obtained at voltages above the breakdown limit ($E_A \geq 75$ V).

Porous titanium oxide and CdSe electrodeposition

Heterogeneously structured titanium oxide substrate was obtained by galvanostatic anodization (G) from a sulfuric acid bath at $I_A \geq 5$ mA cm^{-2}. The oxide layer was well crystallized, consisting of an anatase/rutile mixture (estimated ratio—76:24% A/R) with a network-like morphology. Structured areas of pores with a wide diameter-range, veins of interconnected pores (or craters), and large interpore regions were detected on the oxide film surface (Fig. 5a). Clusters of oriented oxide microcrystals acting as preferential channels for the current flow during the cathodic polarization have been observed in such layers [12]. Such microchannels in the structure of G-TiO_2 are expected to enhance ionic conduction while the pore size and distribution affect nucleation and growth of the CdSe epilayer; in the present case, XRD crystallite size was seen to reach 125 nm. A multiply nucleated CdSe specimen having a finely dispersed aggregate structure is presented in Fig. 5b.

On the whole, the potentiostatic electrodeposition of CdSe on barrier and porous oxide substrates leads to compact overlayers. In order to improve the process, it is necessary to obtain monodispersed TiO_2 pores and to achieve a better control of the CdSe deposition. Highly ordered nanoporous TiO_2 films (Fig. 6a) were obtained by anodization of Ti from H_3PO_4-HF-based solutions (Table 1, P_2). The average size of individual pores was found to be ca. 100 nm. The observed average thickness of the porous film is 2 μm as deduced from the cross section in Fig. 6b. According to XRD analysis, TiO_2 with homogeneously dispersed pores exhibits a dominant crystalline structure of rutile.

To avoid the rapid nucleation and growth of CdSe as well as its inhomogeneous concentration gradient in the nanopores, pulsed electrodeposition was employed. Compared with the constant potential deposition, this technique allows a better control over the deposition parameters [23, 24]. Various combinations of potentials, duty cycles, and frequencies were applied in order to determine an effective pulse plating procedure of CdSe into the titania pores. Pulse deposition for a few coulombs (1–2) electrolysis charge resulted in full coverage of the substrate, while the growth of limited amounts of CdSe partially filling the pores could be attained by single pulse deposition, e.g., at −0.9 V for 0.5 s (Fig. 6c). It should be noted that unlike the typical zinc blend CdSe deposits from an acidic solution, the obtained (by a single deposition pulse) very thin CdSe layer on rutile presented the hexagonal wurtzite structure with preferred (10.0) orientation (Fig. 7). According to EDAX analysis, electrodeposits consisted of different Cd/Se atomic ratios depending on the type and charge of electrolysis, e.g., for single pulsed layer (0.2 C charge), the Cd/Se ratio was close to 1, whereas an increasing excess

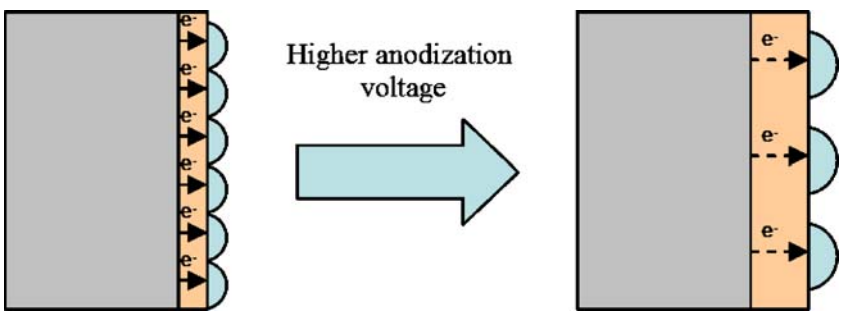

Scheme 1 Growth model for CdSe on barrier titanium oxide substrates prepared at anodization voltages up to 50 V (*left*) and $50 < E_A \leq 100$ V (*right*)

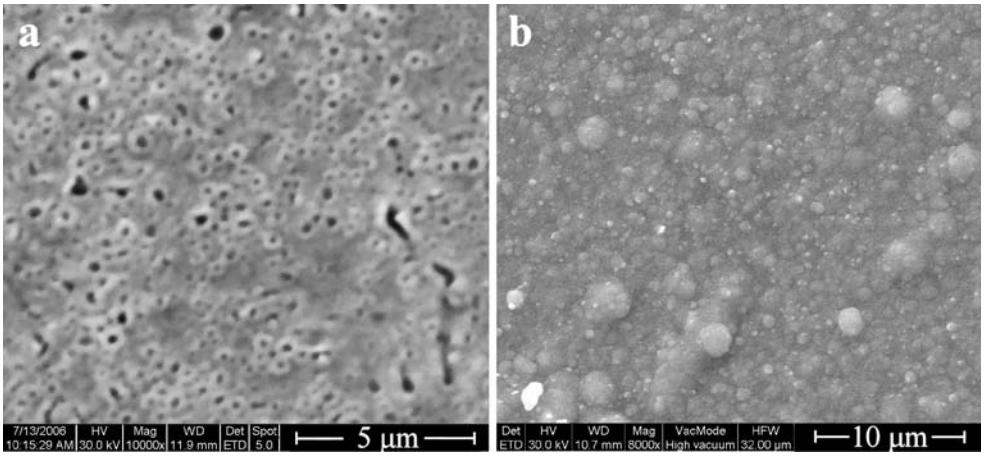

Fig. 5 SEM micrographs of **a** an oxide layer obtained on Ti at I_A=5 mA cm^{-2} from a 1-M H_2SO_4 bath at 25 °C for 3 h and **b** CdSe epilayer prepared at −0.9 V from a typical selenite bath. CdSe crystallite size—125 nm. Estimated oxide phase content ratio—76:24% A/R

of Cd was obtained with the increase of deposition time; for instance, 2 C charge correspond to Cd/Se ≈ 2.

Photoelectrochemical characterization

As-prepared CdSe–titanium oxide systems were tested in a photoelectrochemical cell ($Ti/TiO_x/CdSe/S^{-2}$, S_x^{-2}/Pt) by means of photocurrent spectroscopy and standard photocurrent–potential measurements under green light illumination.

Photocurrent spectroscopy

Representative photocurrent spectroscopy results are given in Fig. 8, implying a strong influence of the substrate on the absorption limit of the photoactive CdSe layer. In contrast to the crystalline porous TiO_2 and Ti substrates, the highly amorphous TiO_x substrates appear to induce growth of CdSe deposits with red-shifted energy bandgaps. As implied by the observed absorption tail (Fig. 8 a), this red shift can be attributed to defect perturbation, usually associated with a Gaussian distribution of states with energies extending into the forbidden gap of CdSe. In fact, a lowering of the measured limit of light absorption from 1.7 eV for CdSe/Ti [20] to about 1.6 eV is observed for all TiO_x substrates anodized at 5, 10, 20, and 50 V. These results were connected to the estimated CdSe XRD crystallite sizes. Since CdSe deposits on TiO_x had much lower crystallite sizes compared to those on Ni and Ti, it becomes evident that there is a relation between CdSe film morphology and PEC behavior. Clearly, smaller crystal size in a cauliflower aggregate environment is related to a more defective structure and in turn to the introduction of more energy states within the bandgap.

Photocurrent voltammetry

Regarding the CdSe deposits on the organized porous TiO_2 substrates, it was found that even small amounts, being deposited by a single pulse, lead to the production of measurable photocurrents. It should be noted that in this case, the coverage of the substrate surface is partial, thus allowing a contact between the electrolyte and the oxide as in dye-sensitized solar cells. Increasing the electrodeposition charge, samples with fully CdSe-covered substrates were prepared and optimized for their photoresponse in the

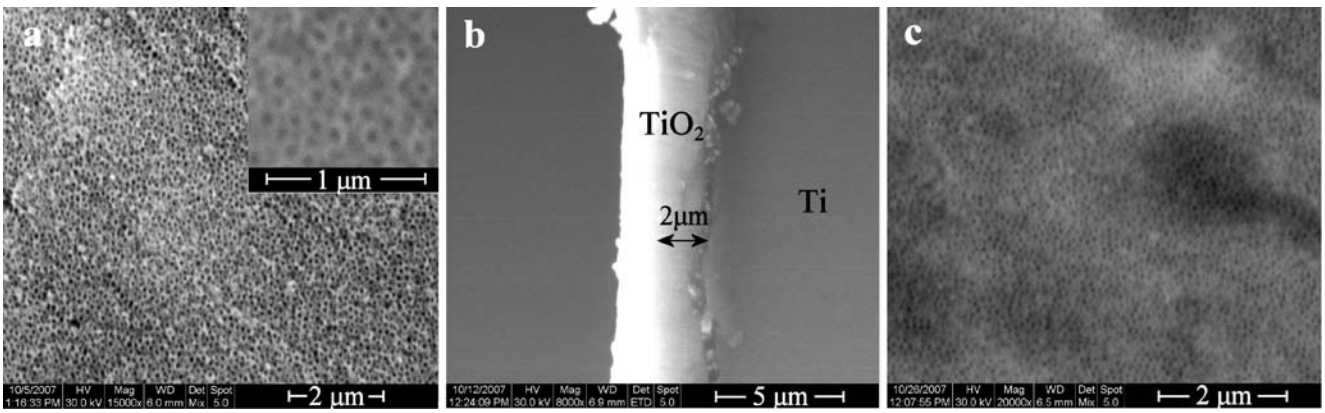

Fig. 6 SEM micrographs of a bare porous oxide layer obtained at 20 V for 3 h (Table 1, P_2): **a** top view in lower and higher (*inset*) magnification, **b** cross section, and **c** the previous layer after deposition of CdSe by a single pulse at −0.9 V for 0.5 s

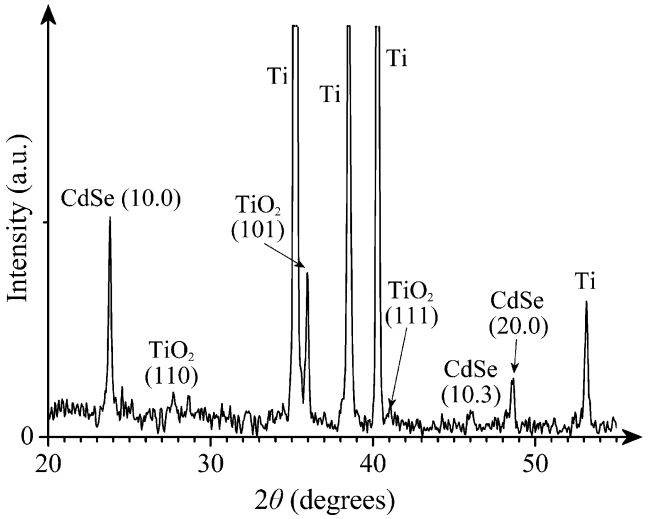

Fig. 7 XRD pattern of deposited CdSe layer by a single pulse at −0.9 V for 0.5 s on the nanoporous Ti oxide

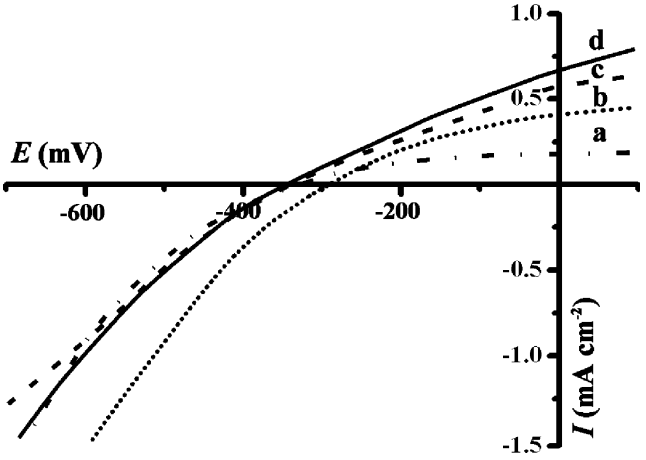

Fig. 9 Photocurrent–potential characteristics in a polysulfide solution under 100 mW cm^{-2} of green light illumination for different CdSe deposition charges on porous TiO_2—0.2 (*a*), 0.5 (*b*), 1.5 (*c*), and 2 C (*d*). Scan rate 10 mV s^{-1}

testing PEC by the application of various pulsed potential profiles. As can be seen on Fig. 9, all samples with deposited amounts from 0.2 to 2 C had photopotentials above −300 mV, while further increase in the charge did not affect the photocurrent. Revealed optimal conditions for improved photoresponse, surpassing the photocurrents obtained by comparable deposits on metallic Ti, thin TiO_x, and nonporous TiO_2 barrier-layer substrates are E_{ON}=−0.9 V, E_{OFF}=0 V, d.c.=75%, ν=0.25 Hz, Q=2 C (a maximum photocurrent shown in Fig. 10).

CdSe deposits on thin TiO_x barrier layers and metallic Ti substrates had similar current–potential characteristics, with open circuit potentials (V_{OC}) around −250 mV vs. Pt and photocurrents of the same magnitude, despite the TiO_x-induced red shift of the energy bandgap. This fact can be attributed to the highly defective structure of the red-shifted samples, inducing increased recombination of the photo-excited carriers. Furthermore, deposits on the porous template show a 100-mV negative shift of V_{OC} and an enhanced photocurrent, compared to the previous samples. Rigid TiO_2 barrier layers (E_A=20 V for 3 h in 1 M H_2SO_4) show almost no photoactivity, underlining the necessity for a porous structure in order to achieve an effective sensitization. It should be noted at this point that similar

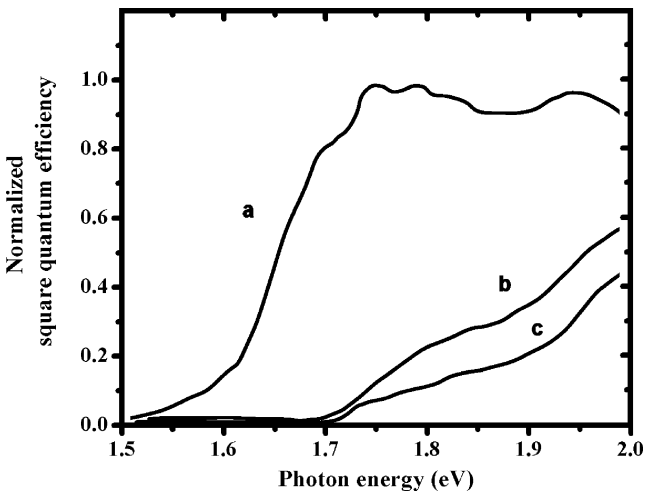

Fig. 8 Square quantum efficiency, normalized to the 2.3-eV value vs. photon energy spectra of CdSe electrodeposits on: *a* potentiostatic barrier oxide layer (anodization at 20 V for 20 min in 1 M H_2SO_4), *b* porous oxide (anodization at 20 V for 3 h in 1 M H_3PO_4–0.5 wt.% HF), and *c* HF-treated Ti

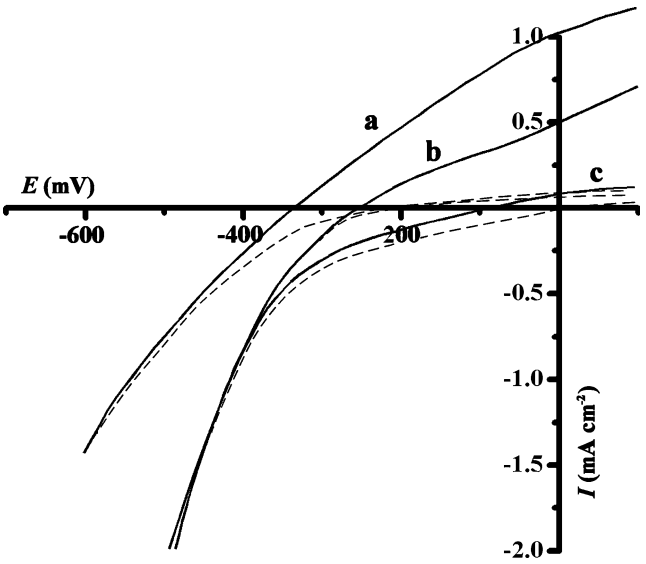

Fig. 10 Photocurrent–potential characteristics of the PEC with three different photoactive electrodes: *a* CdSe on porous TiO_2, *b* CdSe on Ti or thin amorphous TiO_x, and *c* CdSe on rigid TiO_2. *Solid lines*: currents under 100 mW cm^{-2} green light illumination. *Dashed lines*: dark currents

results showing an enhancement of photoactivity due to the introduction of pores in TiO_2 were also reported by authors implementing other sensitizing materials in the form of epilayers [25].

Apart from the negative shift of V_{OC}, the porous substrate also induced a 200-mV negative shift in the photocurrent–onset potential V_{on} (Fig. 10), which may be used as a good approximation of the flat band potential, whose real value is expected actually at a slightly more negative potential. A reason for this shift could be a pore-mediated suppression of the diffusional back-current, thus reducing recombination losses in the bulk CdSe. The CdSe-filled pores might act as channels, in which photo-excited electrons are driven by diffusion into the TiO_2-phase, as in nanostructured TiO_2 electrodes [26], before they can diffuse back to the bulk CdSe phase. The high CdSe/TiO_2 interfacial area provides a large number of interface transition sites, thus making the absorption of photo-excited electrons by the TiO_2 phase more probable.

At the present stage, sensitization effects have been observed only on account of the titanium oxide substrate morphology and not the specific crystallographic structure. Thereby, microheterogeneity of anodized substrates is essential in attaining a sensitization result.

Conclusions

The anodization of Ti metal under various conditions and the electrodeposition of CdSe on the as-prepared oxide layers have been described. CdSe coatings with micro-structures ranging from zinc blend/wurtzite (particulate and cauliflower-like) to (10.0) textured wurtzite layers were obtained on barrier and porous oxide substrates, respectively.

A pulse plating protocol was developed to attain deposition of CdSe on a porous titania template consisting of monodisperse, 100 nm in diameter, pores. For the CdSe/(porous TiO_2)/Ti system, the degree of pore-filling turned out to be important in terms of the optical response, as evaluated by photovoltammetry and photocurrent spectroscopy in polysulfide PEC under green light illumination. A sensitization effect on TiO_2 was evidenced by a negative shift of the flat band potential and a rise in the open circuit potential.

A network-like porous morphology of TiO_2 affording a very thin CdSe coating partially covering the surface appears to be essential for producing a sensitized hetero-junction system, as ensuring high area interface for both the TiO_2/electrolyte and TiO_2/CdSe contacts.

References

1. McEvoy AJ, Grätzel M (1994) Sol Energy Mater Sol Cells 32:221. doi:10.1016/0927-0248(94)90260-7
2. Gratzel M (1994) Renew Energy 5:118. doi:10.1016/0960-1481(94)90361-1
3. Gerischer H, Lübke M (1986) J Electroanal Chem 204:225. doi:10.1016/0022-0728(86)80520-4
4. Mane RS, Roh SJ, Joo O-S, Lokhande CD, Han S-H (2005) Electrochim Acta 50:2453. doi:10.1016/j.electacta.2004.10.075
5. Niitsoo O, Sarkar SK, Pejoux C, Rühle S, Cahen D, Hodes G (2006) J Photochem Photobiol A 181:306. doi:10.1016/j.jphotochem.2005.12.012
6. Toyoda T, Tsuboya I, Shen Q (2005) Mater Sci Eng C 25:853. doi:10.1016/j.msec.2005.07.013
7. Toyoda T, Kobayashi J, Shen Q (2008) Thin Solid Films 516:2426. doi:10.1016/j.tsf.2007.04.143
8. Si H-Y, Sun Z-H, Zhang H-L (2008) Colloids Surf A Physicochem Eng Asp 313–314:604. doi:10.1016/j.colsurfa.2007.04.160
9. Quinn RK, Armstrong NR (1978) J Electrochem Soc 125:1790. doi:10.1149/1.2131295
10. Leitner K, Schultze JW, Stimming U (1986) J Electrochem Soc 133:1561. doi:10.1149/1.2108969
11. Delplancke J-L, Winand R (1988) Electrochim Acta 33:1539. doi:10.1016/0013-4686(88)80223-8
12. Delplancke J-L, Garnier A, Massiani Y, Winand R (1994) Electrochim Acta 39:1281. doi:10.1016/0013-4686(94)E0048-5
13. Beranek R, Hildebrand H, Schmuki P (2003) Electrochem Solid-State Lett 6:B12. doi:10.1149/1.1545192
14. Bauer S, Kleber S, Schmuki P (2006) Electrochem Commun 8:1321. doi:10.1016/j.elecom.2006.05.030
15. Mor GK, Varghese OK, Paulose M, Grimes CA (2005) Adv Funct Mater 15:1291. doi:10.1002/adfm.200500096
16. Shankar K, Mor GK, Fitzgerald A, Grimes CA (2007) J Phys Chem C 111:21. doi:10.1021/jp066352v
17. Tsuchiya H, Macak JM, Taveira L, Balaur E, Ghicov A, Sirotna K, Schmuki P (2005) Electrochem Commun 7:576. doi:10.1016/j.elecom.2005.04.008
18. Yoriya S, Prakasam HE, Varghese OK, Shankar K, Paulose M, Mor GK, Latempa TJ, Grimes CA (2006) Sens Lett 4:334. doi:10.1166/sl.2006.042
19. Bouroushian M, Loizos Z, Spyrellis N (2000) Appl Surf Sci 156:125. doi:10.1016/S0169-4332(99)00487-0
20. Bouroushian M, Charoud-Got J, Loizos Z, Spyrellis N, Maurin G (2001) Thin Solid Films 381:39. doi:10.1016/S0040-6090(00)01687-4
21. Zhang H, Banfield JF (2000) J Phys Chem B 104:3481. doi:10.1021/jp000499j
22. Nauer M, Ernst K, Kautek W, Neumann-Spallart M (2005) Thin Solid Films 489:86. doi:10.1016/j.tsf.2005.05.008
23. Nielsch K, Müller F, Li A-P, Gösele U (2000) Adv Mater 12:582. doi:10.1002/(SICI)1521-4095(200004)12:8<582::AID-ADMA582>3.0.CO;2-3
24. Li L, Yang Y, Huang X, Li G, Zhang L (2005) J Phys Chem B 109:12394. doi:10.1021/jp0511855
25. Sayama K, Oi T, Abe R, Yanagida M, Sugihara H, Iwasaki Y (2006) Sol Energy Mater Sol Cells 90:2429. doi:10.1016/j.solmat.2006.03.028
26. Södergren S, Hagfeldt A, Olsson J, Lindquist S-E (1994) J Phys Chem 98:5552. doi:10.1021/j100072a023